doi:10.1016/j.jmb.2010.04.050 J. Mol. Biol. (2010) 400, 38–51

JMB

Available online at www.sciencedirect.com

ScienceDirect

ELSEVIER

A Divalent Cation Stabilizes the Active Conformation of the *B. subtilis* RNase P·Pre-tRNA Complex: A Role for an Inner-Sphere Metal Ion in RNase P

John Hsieh[1], Kristin S. Koutmou[1], David Rueda[1], Markos Koutmos[2], Nils G. Walter[1] and Carol A. Fierke[1,3]*

[1]*Department of Chemistry, University of Michigan, Ann Arbor, MI 48109, USA*

[2]*Life Sciences Institute, University of Michigan, Ann Arbor, MI 48109, USA*

[3]*Department of Biological Chemistry, University of Michigan, Ann Arbor, MI 48109, USA*

Received 24 February 2010; received in revised form 22 April 2010; accepted 24 April 2010
Available online 29 April 2010

Metal ions interact with RNA to enhance folding, stabilize structure, and, in some cases, facilitate catalysis. Assigning functional roles to specifically bound metal ions presents a major challenge in analyzing the catalytic mechanisms of ribozymes. *Bacillus subtilis* ribonuclease P (RNase P), composed of a catalytically active RNA subunit (PRNA) and a small protein subunit (P protein), catalyzes the 5′-end maturation of precursor tRNAs (pre-tRNAs). Inner-sphere coordination of divalent metal ions to PRNA is essential for catalytic activity but not for the formation of the RNase P·pre-tRNA (enzyme–substrate, ES) complex. Previous studies have demonstrated that this ES complex undergoes an essential conformational change (to the ES* conformer) before the cleavage step. Here, we show that the ES* conformer is stabilized by a high-affinity divalent cation capable of inner-sphere coordination, such as Ca(II) or Mg (II). Additionally, a second, lower-affinity Mg(II) activates cleavage catalyzed by RNase P. Structural changes that occur upon binding Ca (II) to the ES complex were determined by time-resolved Förster resonance energy transfer measurements of the distances between donor–acceptor fluorophores introduced at specific locations on the P protein and pre-tRNA 5′ leader. These data demonstrate that the 5′ leader of pre-tRNA moves 4 to 6 Å closer to the PRNA·P protein interface during the ES-to-ES* transition and suggest that the metal-dependent conformational change reorganizes the bound substrate in the active site to form a catalytically competent ES* complex.

Keywords: RNase P; tRNA processing; conformational change; metals; trFRET

Edited by D. E. Draper

**Corresponding author.* Department of Chemistry, University of Michigan, 930 North University Avenue, Ann Arbor, MI 48109, USA. E-mail address: fierke@umich.edu.

Current addresses: J. Hsieh, Caldera Pharmaceuticals, 278 DP Road, Suite D, Los Alamos, NM 87544, USA; D. Rueda, Department of Chemistry, Wayne State University, 5101 Cass Avenue, Detroit, MI 48202, USA.

Abbreviations used: E, RNase P holoenzyme; PRNA, RNA component of *Bacillus subtilis* RNase P; P, mature tRNA product; P protein, protein component of *B. subtilis* RNase P; pre-tRNA, precursor tRNA; RNase P, ribonuclease P; S/pre-tRNA^{Asp}, *B. subtilis* precursor tRNA^{Asp} substrate; ES, enzyme–substrate/RNase P·pre-tRNA; trFRET, time-resolved Förster resonance energy transfer; Fl, fluorescein; TMR, tetramethylrhodamine; FWHM, full-width at half-maximum; GMPS, guanosine 5′ monothiophosphate.

Introduction

Metal ions interact with RNA to stabilize structure and promote catalysis. The majority of metal ions form non-specific contacts with the negatively charged RNA via electrostatic interactions.[1,2] However, a small number of divalent cations bind to discrete sites in RNA, forming inner-sphere contacts created as a result of ribozyme folding or ligand binding.[3–5] These high-affinity metal binding sites can contribute to RNA catalysis by enhancing ligand binding and/or stabilizing the active conformation and the catalytic transition state.[1,6–9] A large subset of ribozymes require divalent metal ions for catalytic activity, and discerning the precise role of specifically bound metal ions in the mechanisms of ribozymes remains a formidable challenge in the field of RNA biochemistry.[1,6,10,11]

Nuclear ribonuclease P (RNase P) is a highly conserved RNA-based endonuclease found in all three kingdoms of life that is responsible for catalyzing the hydrolysis of a phosphodiester bond in precursor tRNA (pre-tRNA) to yield mature tRNA.[9,12,13] Bacterial RNase P enzymes are composed of a catalytically active RNA subunit (RNA component of *B. subtilis* RNase P, PRNA) and a small protein subunit (protein component of *B. subtilis* RNase P, P protein) essential for activity *in vivo*.[9,13] Significant progress has been made in the last 5 years toward understanding the structure of RNase P. High-resolution structures have been solved for PRNA (from *Bacillus stearothermophilus* and *Thermotoga maritima*)[4,14,15] and P protein (from *Bacillus subtilis*, *Staphylococcus aureus*, and *T. maritima*).[16–18] However, there are still no high-resolution structural data for either the holoenzyme (PRNA·P protein) or a complex with bound pre-tRNA. Therefore, information on these catalytically relevant structures is limited to models derived from biochemical and biophysical studies.[19–22]

Recent transient kinetic studies revealed a previously masked step in the kinetic mechanism of RNase P: a conformational change following pre-tRNA association with RNase P and preceding cleavage (Scheme 1).[23] In the two-step association mechanism, pre-tRNA binds to RNase P with a bimolecular rate constant that is near the diffusion limit and is independent of the length of the pre-tRNA leader. Following formation of this initial enzyme–substrate (ES) complex, a unimolecular conformational change that enhances the affinity of RNase P for pre-tRNA occurs. This new RNase P·pre-tRNA conformer (ES*) is stabilized by increasing the pre-tRNA leader length from 2 to 4 nucleotides such that an optimal pre-tRNA leader–P protein interaction forms.[23,24] Furthermore, this conformational change is the rate-limiting step for cleavage at high pH and has been proposed to align essential functional groups at the active site to enhance efficient cleavage of pre-tRNA.[23] However, the structural alterations that accompany this conformational change have not been elucidated.

$$E + S \underset{k_{-1}}{\overset{k_1}{\rightleftharpoons}} ES \underset{k_{-2}}{\overset{k_2}{\rightleftharpoons}} ES^* \xrightarrow{k_3} ELP \xrightarrow{k_4} E + L + P$$

Scheme 1. Minimal kinetic mechanism for RNase P.[23] E is RNase P, S is pre-tRNA^{Asp}, P is tRNA, and L is the 5′-leader product. In summary, substrate binding (k_1, k_{-1}) is followed by a conformational change (k_2, k_{-2}) that precedes substrate cleavage (k_3) and product release (k_4).

Cations interact with RNase P to stabilize RNA folding, ligand binding, and catalytic activity.[9,12,13,25] Catalysis of pre-tRNA cleavage by RNase P requires at least one divalent cation capable of forming inner-sphere coordination, such as Mg(II), Mn(II), Zn(II), or Ca(II).[26] However, the PRNA·P protein and ES complexes form in the presence of $Co(NH_3)_6$(III), an exchange-inert $Mg(II)\cdot(H_2O)_6$ mimic,[26] demonstrating that inner-sphere contacts with metal ions are not essential for either folding or ligand binding. One proposal for the catalytic function of an inner-sphere metal ion, supported by kinetic isotope effect experiments, is that a metal hydroxide serves as the nucleophile in RNase P-catalyzed phosphodiester-bond cleavage.[27] In addition to directly participating in catalysis, inner-sphere metal ions may also enhance RNase P activity by stabilizing the active enzyme structure.[28,29] A variety of structural and biochemical data implicate nucleotides in the catalytic domain of PRNA, particularly helix P4, as binding sites for catalytically important metal ions.[4,30–35] Recently, NMR and X-ray absorption spectroscopy of a helix P4 mimic have identified an inner-sphere metal site at the conserved tandem guanosines adjacent to a bulged uridine in P4.[36,37] However, the precise function and location of the inner-sphere metal ions bound to RNase P remain unclear.

Here, we demonstrate that an inner-sphere metal ion is important for stabilizing the conformational change in the ES complex that precedes phosphodiester-bond cleavage. For these experiments, the ES complex was preformed in the presence of $Co(NH_3)_6$ (III) and the reaction was initiated by addition of divalent metal ions. Measurements of the kinetics and thermodynamics of the conformational change using fluorescent techniques reveal that Ca(II) or Mg (II) stabilizes the active conformer of the ES complex by >10-fold with an apparent micromolar affinity. Furthermore, a second Mg(II) ion with considerably weaker affinity is required to activate cleavage, demonstrating the existence of at least two classes of catalytically important Mg(II) ions. Time-resolved Förster resonance energy transfer (trFRET) studies performed as a function of Ca(II) concentration reveal that during the isomerization of the ES complex the pre-tRNA leader repositions relative to the protein subunit. These data suggest that in the metal-stabilized conformational change, the pre-tRNA leader may "dock" into the active site of RNase P to form a catalytically active complex. Furthermore, we propose that this conformational change may also serve as a proofreading step to enhance substrate selectivity.

Results

An inner-sphere metal ion enhances pre-tRNA affinity

Although divalent metal ions capable of forming inner-sphere contacts are required to activate RNase P catalysis, they are not essential for substrate binding.[26] Nonetheless, the affinity of *B. subtilis* RNase P for pre-tRNA and tRNA are increased by monovalent and divalent cations.[24,38,39] To evaluate the potential contribution of inner-sphere contacts to substrate affinity, we compared the $K_{d,obs}$ for pre-tRNA in the presence of saturating concentrations of Ca(II) or $Co(NH_3)_6$(III)[26] (Fig. 1a). The apparent association constant for 5′-fluorescein-labeled *B. subtilis* pre-tRNA^{Asp} (Fl-pre-tRNA) possessing a 5-nucleotide leader with *B. subtilis* RNase P was measured from an increase in fluorescence intensity upon addition of RNase P.[20,23,40] The value of $K_{d,obs}$ decreases from 28±6 nM in 2 mM $Co(NH_3)_6$(III) to 0.50±0.03 nM in 10 mM Ca(II), with the ionic strength maintained with KCl, indicating that the ES complex is stabilized more than 50-fold by calcium relative to cobalt hexammine.

Similarly, the ES complex formed in the presence of cobalt hexammine is stabilized by the addition of Ca(II) (Fig. 1b). In fact, the value of $K_{d,obs}$ for pre-tRNA in cobalt hexammine decreases 10-fold from 28±6 to 2.7±0.5 nM upon addition of 1 mM $CaCl_2$. The value of $K_{d,obs}$ has an hyperbolic dependence on the concentration of calcium with an apparent dissociation constant for Ca(II) of 40±10 μM, as determined by fitting a binding isotherm to these data (Eq. (2), $n=1$; see Materials and Methods); this value decreases modestly to 30±10 μM when the equation includes a term for Ca(II) binding to RNase P holoenzyme (E) with weak affinity of 500±300 μM (Eq. (3)). The value of $K_{d,app}$ is virtually unchanged when the data are fit with a Hill equation including cooperative binding of calcium ($n=0.9\pm0.3$). These results indicate that at least one class of Ca(II) ions binds with high affinity to stabilize the RNase P·substrate complex relative to the uncomplexed RNase P and pre-tRNA in cobalt hexammine (Scheme 2). Cobalt hexammine only forms outer-sphere interactions with RNA, and the higher charge of the $Co(NH_3)_6$(III) ion enhances this electrostatic interaction compared with divalent cations.[41] Therefore, the observation that Ca(II) binds with high affinity even in the presence of

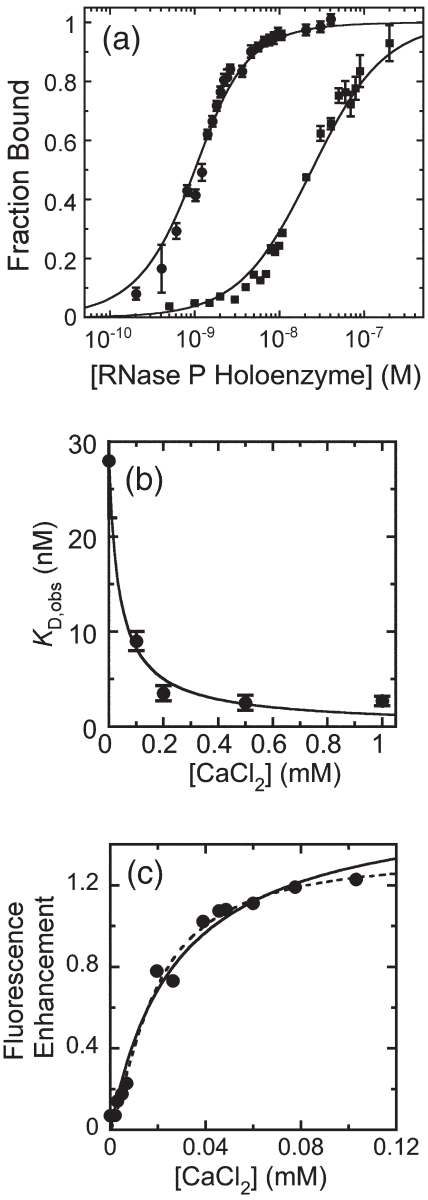

Fig. 1. Calcium dependence of the binding affinity of RNase P for Fl-pre-tRNA. (a) Association of Fl-pre-tRNA with a 5-nucleotide leader (Fl-pre-tRNA) to *B. subtilis* RNase P was observed by enhancement of fluorescence intensity ($\lambda_{ex}=488$ nm; $\lambda_{em}=524$ nm). Fluorescence titrations of Fl-pre-tRNA (1 nM) with RNase P in either 2 mM $Co(NH_3)_6Cl_3$/150 mM KCl (■) or 10 mM $CaCl_2$/20 mM DTT (●) in 50 mM Tris and 50 mM Mes, pH 6.0, at 25 °C are shown. The apparent dissociation constants for Fl-pre-tRNA were obtained by fitting Eq. (1) to these binding isotherms, yielding values for $K_{d,obs}$ of 28±6 nM in 2 mM cobalt hexammine and 0.50±0.03 nM in 10 mM calcium. (b) The apparent dissociation constant ($K_{d,obs}$) for the RNase P·Fl-pre-tRNA complex was determined as a function of $CaCl_2$ concentration (0–1 mM) from changes in the Fl fluorescence intensity in 2 mM $Co(NH_3)_6Cl_3$, 189 mM KCl, 50 mM Tris, and 50 mM Mes, pH 6.0, at 25 °C. The value of 40±10 μM for the apparent calcium dissociation constant ($K_{Ca,obs}$) of the RNase P·Fl-tR5·Ca complex was determined from fitting Eq. (2) to these data. (c) Titration of calcium into the preformed RNase P·Fl-pre-tRNA complex (300 nM RNase P, 15 nM pre-tRNA in 2 mM $Co(NH_3)_6Cl_3$, 20 mM DTT, 380 mM KCl, 50 mM Tris, and 50 mM Mes, pH 6.0, at 25 °C) increases the intensity of the Fl fluorescence. The apparent calcium dissociation constant of the RNase P·Ca·Fl-pre-tRNA complex is determined from fitting either a non-cooperative ($K_{Ca,obs}=28\pm5$ μM; $n=1$; continuous line) or a cooperative ($K_{Ca,obs}=19\pm3$ μM; $n=1.4\pm0.2$; dashed line) binding isotherm to these data.

$$E + S + Ca(II) \rightleftarrows E{\bullet}S + Ca(II) \rightleftarrows E{\bullet}S_{Ca(II)}$$

Scheme 2. Pre-tRNA affinity is coupled to calcium binding in cobalt hexammine. E is RNase P, and S is pre-tRNA^{Asp}.

2 mM $Co(NH_3)_6$(III) suggests that Ca(II) forms inner-sphere contacts with the ES complex.

To further examine the calcium affinity, we titrated Ca(II) into a solution containing the RNase P·Fl-pre-tRNA complex (>90% bound) in 2 mM $Co(NH_3)_6$(III) (Fig. 1c). The fluorescence intensity increases with a hyperbolic dependence on the Ca(II) concentration with an apparent dissociation constant for Ca(II) ($K_{Ca,app}$) of 28±5 μM. A model allowing for a cooperative dependence of $K_{Ca,app}$ on the calcium concentration leads to a modestly better fit of these data with a value for $K_{Ca,app}$ of 19±3 μM (n=1.4±0.2). A value of n larger than 1 could reflect either more than one class of Ca(II) ions stabilizing the RNase P·substrate complex or variations in the concentration of "free" Ca(II) relative to "total" Ca (II) during the titration due to non-specific interactions with RNA. Furthermore, the increase in the fluorescence intensity upon calcium binding to the RNase P·substrate complex indicates that the environment, and perhaps the position, of the Fl at the 5′ end of pre-tRNA is altered. In summary, these results demonstrate that at least one class of high-affinity Ca(II) ions stabilizes the RNase P·substrate complex (Scheme 2).

Calcium ions stabilize a conformational change in the ES complex

Recent stopped-flow studies of pre-tRNA^{Asp} binding to *B. subtilis* RNase P in Ca(II) or Mg(II) demonstrated biphasic kinetic traces consistent with a two-step association mechanism in which an ES encounter complex is formed, followed by a unimolecular isomerization to an ES* complex.[23] The calcium-dependent enhancement of the affinity of RNase P for pre-tRNA (Fig. 1) could be caused by calcium binding to either or both of these complexes. To address this question, we analyzed the calcium dependence of the pre-tRNA association kinetics, monitoring FRET between a donor–acceptor pair attached to the P protein subunit (tetramethylrhodamine, TMR) of RNase P and the 5′ end of pre-tRNA (Fl). Unexpectedly, when TMR-RNase P was mixed with Fl-pre-tRNA in the presence of Co $(NH_3)_6$(III), only a single fluorescence phase was observed (Fig. 2a). The observed rate constant of this phase is linearly dependent on the RNase P concentration (Fig. 2b) with a second-order rate constant of 2.0±0.2 μM^{-1} s^{-1}, modestly slower than values for the pre-tRNA association rate constant (4.6±0.2 μM^{-1} s^{-1}) measured in the presence of either 1 mM Ca(II)/2 mM $Co(NH_3)_6$(III) or 10 mM Ca(II).[23] Therefore, the single phase observed in Co $(NH_3)_6$(III) alone reflects the association of RNase P and pre-tRNA to form a bound complex.

The absence of a second phase in the pre-tRNA association kinetics in $Co(NH_3)_6$(III) is most simply explained by either destabilization of the ES* conformer relative to ES so that it is not significantly populated or enhancement of the rate constant for isomerization of ES to ES* such that it is faster than the rate of formation of ES. To distinguish between

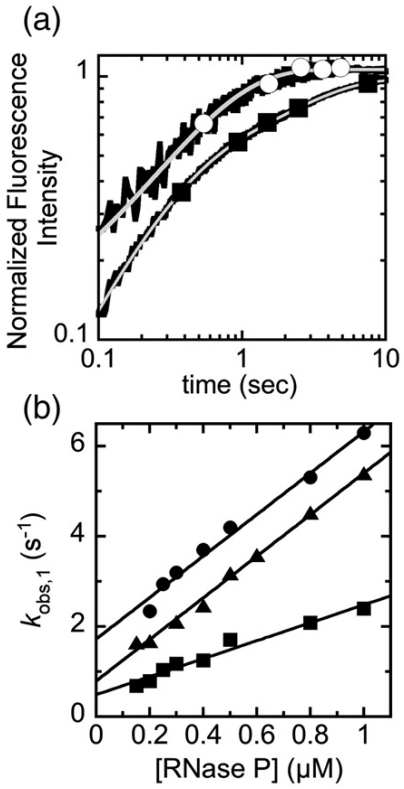

Fig. 2. Fluorescence stopped-flow kinetic measurements of pre-tRNA binding to RNase P. The kinetics of Fl-pre-tRNA binding to TMR-RNase P were monitored by fluorescence resonance energy transfer from Fl to TMR (λ_{ex}=488 nm; λ_{em},>600 nm). Fl-pre-tRNA is labeled at the 5′ terminus with Fl, and the protein subunit of RNase P is labeled with TMR. (a) Representative fluorescence transients observed upon mixing TMR-RNase P with Fl-pre-tRNA (final concentration of 35–50 nM 5′-Fl-pre-tRNA, 200 nM RNase P, 189 mM KCl, 50 mM Tris, and 50 mM Mes, pH 6.0, at 25 °C) with 2 mM cobalt hexammine alone (○) and with 0.5 mM $CaCl_2$ added (■). The smooth curve superimposed on the time course (white line) is the best fit to the data. In cobalt hexammine alone, the data are fit with a single exponential, k_{obs}=1.6±0.3 s^{-1}, while the data in the presence of $CaCl_2$ are best described by two exponential phases, $k_{obs,1}$=3.1±0.1 s^{-1} and $k_{obs,2}$=0.54±0.01 s^{-1}, as previously reported.[23] (b) The observed association rate constants ($k_{obs,1}$) were measured at varying concentrations of TMR-RNase P in 2 mM cobalt hexammine (■), 2 mM cobalt hexammine with 1 mM $CaCl_2$ (●), or 10 mM $CaCl_2$ (▲). The binding kinetics in 10 mM $CaCl_2$ were taken from the work of Hsieh and Fierke.[23] The linear least-squares fit to the dependence of $k_{obs,1}$ on the concentration of RNase P yields the bimolecular association rate constants of 2.0±0.2 μM^{-1} s^{-1} (■), 4.6±0.1 μM^{-1} s^{-1} (●), and 4.6±0.2 μM^{-1} s^{-1} (▲) for these different solution conditions.

these possibilities, we measured the FRET time course upon mixing the ES complex formed in 2 mM $Co(NH_3)_6$(III) with 1 mM Ca(II) (Fig. 3a). We observed an increase in fluorescence with an observed rate constant of 0.79±0.03 s^{-1}, slightly faster than the rate constant for the conformational change previously measured in 10 mM Ca(II) (k_{obs}=0.43±0.02 s^{-1}).[23] Therefore, we conclude that the fluorescent enhancement observed upon mixing the RNase P·pre-tRNA complex formed in cobalt hexammine with Ca(II) reflects the formation of the ES* conformer. Furthermore, both the observed rate constant (k_{obs}) and the amplitude of the kinetic transient observed after mixing ES with $CaCl_2$ in 2 mM cobalt hexammine have a hyperbolic dependence on the concentration of Ca(II), with values for $K_{1/2,app}$ of 110±20 and 50±10 μM, respectively. This saturation behavior indicates that the fluorescence change not only measures the association of calcium with ES but also reflects a unimolecular step, such as a conformational change. These data demonstrate that Ca(II) enhances the affinity of RNase P for pre-tRNA by stabilizing ES* relative to ES. Therefore, the conformational change is coupled to an increase in calcium affinity (Scheme 2). Furthermore, the $K_{1/2,app}$ for the calcium-dependent activation of the conformational change increases to 230±20 and 700± 200 μM as the concentration of cobalt hexammine decreases to 1.5 and 1.0 mM, respectively (data not shown). These data indicate that cobalt hexammine and calcium act synergistically, not competitively, to stabilize the ES* complex. However, the $K_{1/2,app}$ for calcium estimated from the kinetic data at 2 mM cobalt hexammine is 2- to 4-fold higher than the values of $K_{Ca,app}$ estimated from the calcium-dependent enhancement of pre-tRNA affinity (Fig. 1c). This discrepancy could arise from changes in the "free" concentrations of Ca(II) and/or cobalt hexammine due to binding to RNase P RNA, Ca(II) binding to E or ES in addition to ES* at high Ca(II) concentrations, and/or kinetic perturbation of the values of $K_{1/2,app}$ for Ca(II).

Two classes of magnesium ions enhance catalytic activity of RNase P

Although RNase P has higher catalytic activity in the presence of the physiological cofactor Mg(II),[39] the pre-tRNA binding mechanism for RNase P is similar at saturating Mg(II) and Ca(II) concentrations with a comparable rate constant for the conformational change.[23] This conformational change is the rate-limiting step at high pH for turnover in magnesium.[23] To analyze the dependence of the conformational change on the magnesium concentration, we measured the change in FRET efficiency upon adding $MgCl_2$ to the TMR-RNase P·Fl-pre-tRNA complex formed in $Co(NH_3)_6$ (III) using stopped-flow techniques (Fig. 4a). At 1 mM Mg(II), the FRET signal *increases* with an observed rate constant of 0.96±0.03 s^{-1} (Fig. 4a), consistent with the formation of the ES* conformer and inconsistent with pre-tRNA cleavage. Rapid-

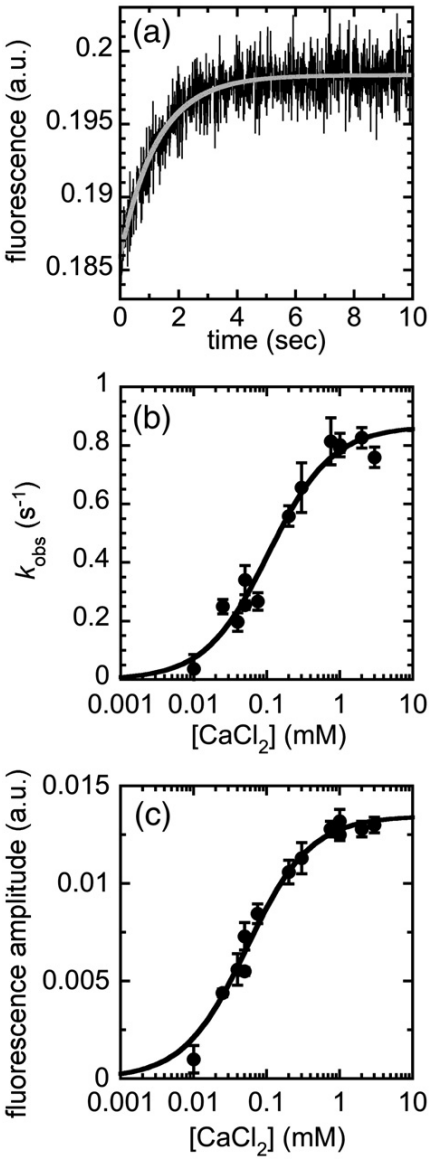

Fig. 3. Conformational change in the ES complex coupled to calcium binding observed by stopped-flow fluorescence spectroscopy. (a) The TMR-RNase P·Fl-pre-tRNA (ES) complex formed in 2 mM cobalt hexammine [2 mM $Co(NH_3)_6Cl_3$, 189 mM KCl 50 mM Tris, 50 mM Mes, pH 6.0, at 25 °C] was mixed with varying concentrations of $CaCl_2$, and the FRET from Fl to TMR was measured as described in the legend to Fig. 2. A representative trace for mixing the ES complex (35 nM 5′-Fl-tR5, 125 nM RNase P) with 1 mM $CaCl_2$ in 2 mM cobalt hexammine is shown. The smooth curve superimposed on the time course is the best single-exponential fit to the data with k_{obs}=0.79±0.03 s^{-1}. (b) The observed rate constant for the fluorescent transient observed upon mixing ES with Ca depends on the concentration of $CaCl_2$. The smooth curve is the least-squares fit of a rectangular hyperbola to these data and yields k_{max}=0.9±0.1 s^{-1} and $K_{1/2}$ =110±20 μM for $CaCl_2$. (c) The amplitude of the fluorescent transient observed upon mixing ES with Ca depends on the concentration of $CaCl_2$. A least-squares fit of a rectangular hyperbola to these data yields a $K_{1/2}$ of 50±10 μM for $CaCl_2$.

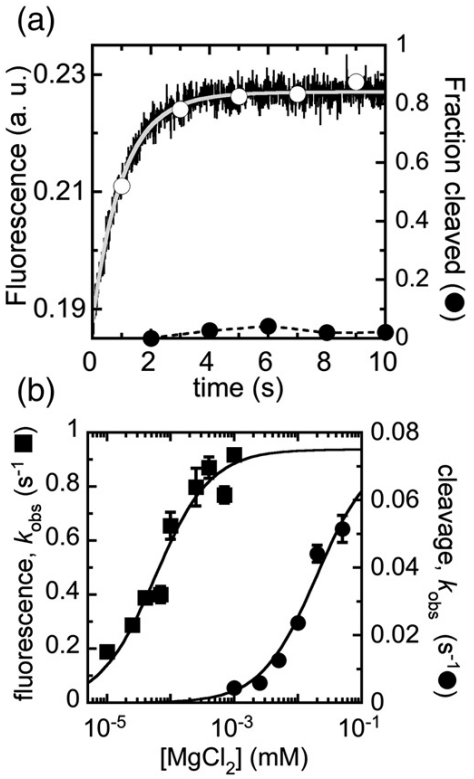

Fig. 4. Kinetic studies of Mg(II) binding to the ES complex. (a) Kinetics of the conformational change and pre-tRNA cleavage after mixing the TMR-RNase P·Fl-pre-tRNA (ES) complex with $MgCl_2$. The ES complex formed in 2 mM cobalt hexammine was mixed with 1 mM $MgCl_2$ (final concentration of 35 nM Fl-pre-tRNA, 125 nM TMR-RNase P, 1 mM $MgCl_2$, 2 mM cobalt hexammine, 189 mM KCl, 50 mM Tris, and 50 mM Mes, pH 6.0, at 25 °C). The kinetics of the conformational change (○) were measured from fluorescence energy transfer, as described in the legend to Fig. 2. The smooth curve superimposed on the time course is the best single-exponential fit to the data with $k_{obs}^{fluorescence} = 0.96 \pm 0.03$ s^{-1}. The kinetics of Fl-pre-tRNA cleavage (●) were performed by using a chemical quench-flow apparatus, and the formation of the 5′ leader containing Fl was analyzed by denaturing PAGE and PhosphoImager analysis, as described in Materials and Methods. Under these conditions, <5% of Fl-pre-tRNA is cleaved in 90 s. (b) The $MgCl_2$ dependence of the observed rate constants for the conformational change $k_{obs}^{fluorescence}$ (■) and for the pre-tRNA cleavage $k_{obs}^{cleavage}$ (●). The least-squares fit of a rectangular hyperbola to these data yields $k_{max}^{fluorescence} = 0.94 \pm 0.05$ s^{-1} with $K_{1/2} = 60 \pm 10$ μM and $k_{max}^{cleavage} = 0.08 \pm 0.01$ s^{-1} with $K_{1/2} = 19 \pm 6$ mM.

quench methods confirm this conclusion by demonstrating that <5% of pre-tRNA is cleaved after 10 s, which is >10 half-times for the fluorescent transient, under these reaction conditions (Fig. 4a). The observed rate constant for the fluorescent transient, reflecting the conformational change, has a hyperbolic dependence on the concentration of Mg (II) (Fig. 4b) with a rate constant of 0.94 ± 0.05 s^{-1} at saturating Mg(II) and a $K_{1/2}$ value of 60 ± 10 μM, similar to the values measured in Ca(II). The observed rate constant for pre-tRNA cleavage also has a hyperbolic dependence on the Mg(II) concentration; however, the maximal rate constant, 0.08 ± 0.01 s^{-1}, is reduced and the $K_{1/2}$ for activation of cleavage by Mg(II) is much higher, 19 ± 6 mM. This value of $K_{1/2}^{Mg}$ is comparable with previous measurements in cobalt hexammine,[26] but the value of k_{max} is decreased by ~2-fold due to the decrease in temperature from 37 to 25 °C. These kinetic data indicate that RNase P in cobalt hexammine requires two classes of Mg(II) ions to activate catalytic activity: a high-affinity Mg(II) cation that stabilizes the active ES* complex prior to cleavage and a weakly bound Mg(II) that enhances the cleavage step.

In summary, both Mg(II) and Ca(II) stabilize the ES* conformer relative to the encounter complex in the presence of cobalt hexammine with a similar observed rate constant for isomerization. These data are consistent with a model in which the conformational change is coupled to the formation of a high-affinity inner-sphere metal-ion site. Divalent cations, such as Mg(II) and Ca(II), have higher affinity to this binding site in the ES* conformer compared with ES, stabilizing the ES* conformer by forming ES*Me(II) (Scheme 2). Cobalt hexammine does not compete for this high-affinity metal site; instead, this cation further stabilizes the ES*Me(II) complex, presumably by binding to other regions of PRNA. Since both Mg (II) and Ca(II) are capable of forming inner-sphere contacts, while $Co(NH_3)_6$(III) is exchange-inert, these data suggest that the high-affinity divalent cation binding site in the ES* complex includes one or more inner-sphere interactions. However, our current data do not distinguish whether the divalent cation binds before the conformational change to facilitate this step or after the conformational change to stabilize this conformer (Scheme 3).

The pre-tRNA 5′ leader is repositioned in the Ca(II)-stabilized ES* state

The observed changes in the FRET and fluorescence intensity signals during the unimolecular conformational change step suggest that the 5′ leader is repositioned during this reaction. Previously, the structure of the 5′ leader of pre-tRNA

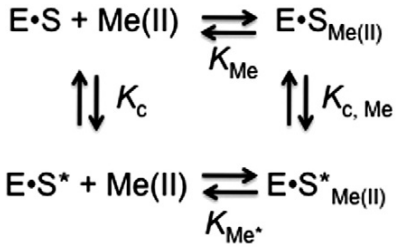

Scheme 3. Divalent cations stabilize the ES* conformation of RNase P. E is RNase P, S is pre-tRNA^{Asp}, Me(II) is either Ca(II) or Mg(II), and E·S* denotes an alternate conformer of the ES complex that is stabilized by divalent cations ($K_{c,Me} > K_c$ and $K_{Me} > K_{Me*}$).

interacting with the *B. subtilis* P protein in the ES complex was modeled using distances between the 5′ end of pre-tRNA and discrete P protein residues obtained by trFRET techniques.[20] These data were collected in the presence of saturating Ca(II) (20 mM), so this model reflects the structure of the active ES* state. To probe the structural changes that occur in the ES-to-ES* transformation, we used trFRET to measure changes in distances between discrete positions in the P protein and the 5′ end of pre-tRNA in $Co(NH_3)_6$(III) as a function of the Ca (II) concentration. For this purpose, we used Fl-pre-tRNA as the FRET donor paired with a TMR-labeled single-cysteine variant of the P protein (E40C, L94C, Y113C) as the FRET acceptor (see Materials and Methods). Fluorescence labels at these positions minimally alter the catalytic activity and affinity of RNase P for pre-tRNA (<2-fold).[20,21] The trFRET measurements provide a distribution of distances that is characterized by both a mean distance between the fluorophores and a full-width at half-maximum (FWHM).

For each of the donor–acceptor pairs, the distance distributions measured by trFRET vary with the calcium concentration, demonstrating that the 5′ leader is repositioned relative to the P protein upon the formation of the Ca(II)-stabilized ES* complex (Fig. 5). The anisotropy of the fluorophores varies by ≤12% (Table S1) as a function of Ca(II), demonstrating that the changes in trFRET can be interpreted mainly as distance changes. The distance between Fl at the 5′ end of pre-tRNA and TMR attached at E40C has a hyperbolic dependence on the Ca(II) concentration; at saturating Ca(II), this distance *decreases* by 4.8±0.4 Å (Fig. 5a). A similar change in the donor–acceptor distance is observed for addition of 0.1 mM $CaCl_2$, $Ca(acetate)_2$, and $MgCl_2$ but not 5 mM NaCl or KCl (Table S1). Residue 40 is near the N-terminus and the α-helix on the front face of the P protein (Fig. 6). In contrast, the distances between Fl at the 5′ end of pre-tRNA and TMR labeled at L94C and Y113C *increase* by 6.0±0.4 and 6.0±0.6 Å, respectively, at saturating calcium (Fig. 5b and c). These positions are located on the opposite side of the protein, in close proximity to the central cleft β-sheet and RNR motif (Fig. 6). For each donor–acceptor pair, the FWHM determined from the trFRET data also varies with the calcium concentration, suggesting changes in the dynamics of the pre-tRNA leader as well (see Supporting Information; Fig. S1). Furthermore, for each labeled position in the P protein, the calcium dependence of the metal-stabilized structural change, determined from fitting a binding isotherm ($n=1$) to these data, is comparable, with $K_{1/2,app}$ values of 20–25 μM for both the distance distributions and the FWHM. The fits of the calcium dependence of the distance distributions with the TMR donor attached to E40C and Y113C are improved slightly by allowing the Hill coefficient to vary (0.7–1.6); however, the values for the distance change and the $K_{1/2,app}$ values are not significantly altered. Together, these data suggest a model in which a single high-affinity metal ion (or

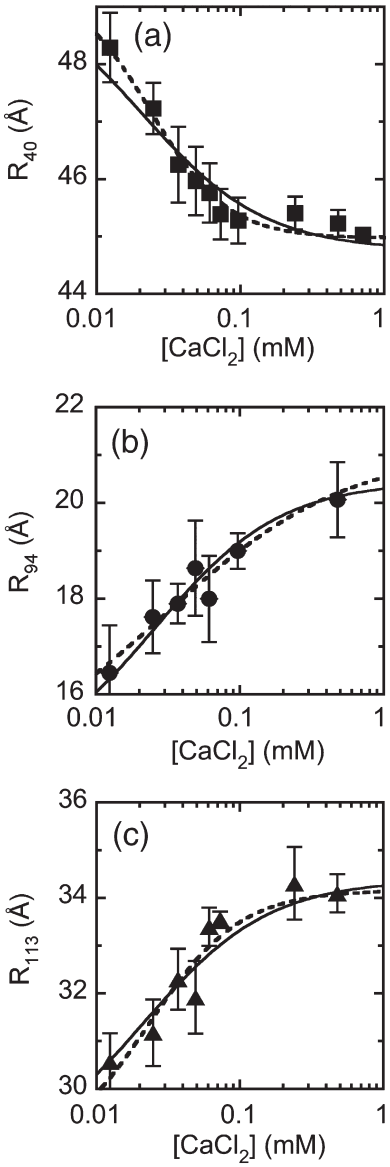

Fig. 5. trFRET distance measurements of the TMR-RNase P·Fl-pre-tRNA complex to monitor structural changes that accompany Ca(II) binding. The relative distances between Fl-TMR donor–acceptor pairs in the TMR-RNase P·Fl-pre-tRNA complex were measured by trFRET as a function of calcium concentration. The ES complex was formed by pre-incubating Fl-pre-tRNA (250–500 nM) with RNase P (1–1.5 μM) in 2 mM cobalt hexammine, 189 mM KCl, 50 mM Tris, and 50 mM Mes, pH 6.0, at 25 °C. The mean donor–acceptor distances for RNase P·Fl-pre-tRNA formed with the TMR-labeled E40C (a), L94C (b), and Y113C (c) single-cysteine variants of the P protein subunit are shown as a function of calcium concentration. Donor-only experiments using unlabeled RNase P with bound Fl-pre-RNA were performed in parallel. Error bars arise from at least three independent assays. Either a non-cooperative (continuous line; $n=1$) or a cooperative (dashed line; n = variable, 0.7–1.6) binding isotherm is fit to the data.

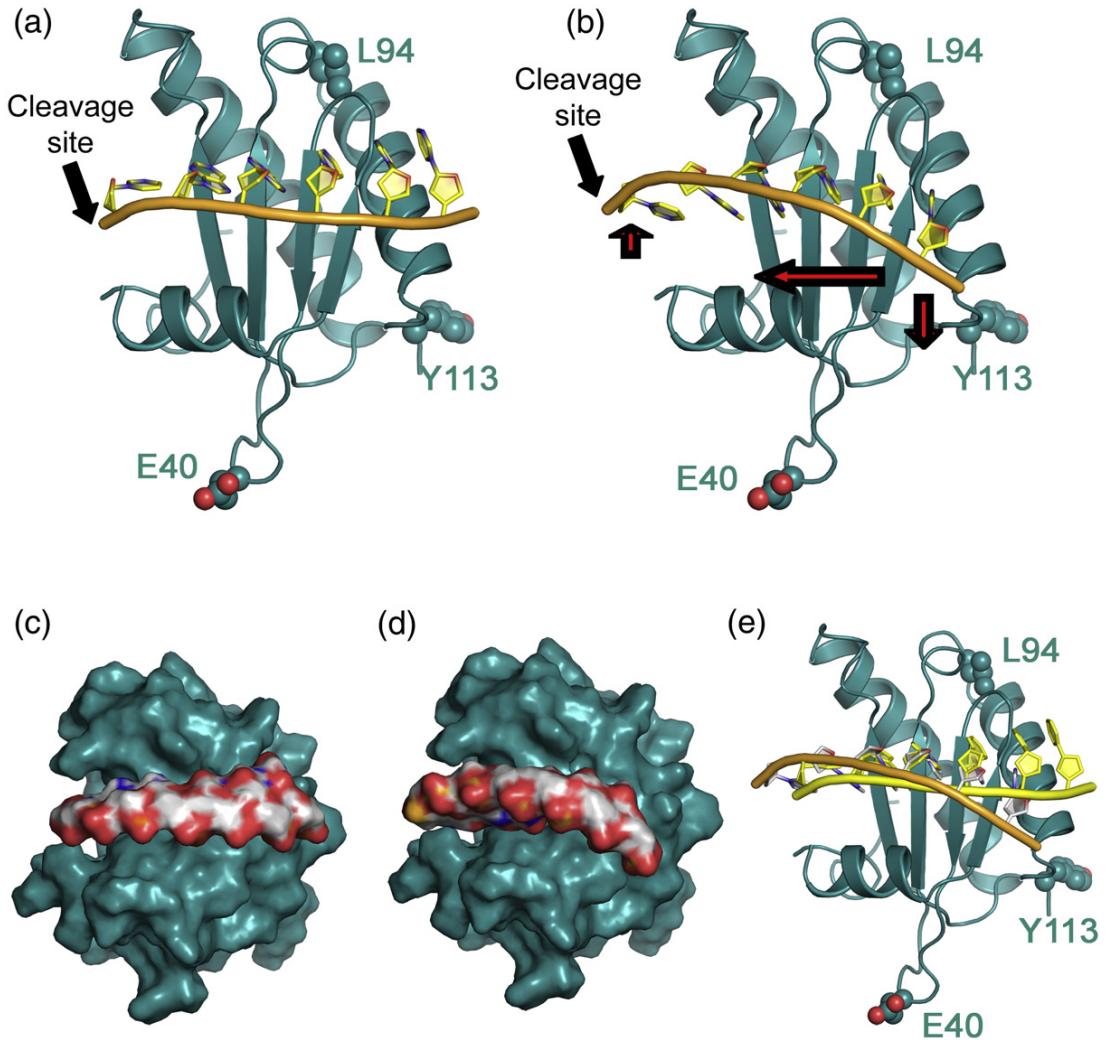

Fig. 6. Models of the ES and ES* complexes. The P protein is displayed in cyan (a–e), and the pre-tRNA 5′ leader is shown in yellow (a–b). Panels (c) and (d) are space-filling depictions of the models displayed in panels (a) and (b), respectively. The P protein positions labeled with the TMR acceptor fluorophore (E40, L94, and Y113) are highlighted in (a), (b), and (e). An overlay of the 5′ leader in the ES (yellow) and ES* (orange) complexes is shown in (e). The movement of the 5′ leader in the ES* (b, d) complex relative to the ES (a, c) complex is shown in red cartoon arrows in (b).

class of metal ions) binds to stabilize an altered conformation of the ES complex where the 5′ leader is repositioned relative to the P protein subunit in the ES* complex (Fig. 6).

Discussion

Assigning functional roles to the handful of metal ions that bind to specific sites in ribozymes presents a longstanding challenge in the study of catalytic RNAs such as RNase P. Although divalent cations enhance interactions of RNase P RNA with both the protein subunit[42] and pre-tRNA[38] and stabilize the PRNA fold,[29] these cations function mainly by outer-sphere electrostatic interactions, as indicated by the ability of cobalt hexammine to fulfill these roles. However, at least one specifically bound inner-sphere metal ion is essential for activating catalysis of phosphodiester-bond cleavage by RNase P.[26] Magnesium hydroxide has been proposed as the catalytic nucleophile,[27] and this or an additional divalent cation is also proposed to interact with the scissile phosphodiester of pre-tRNA.[43] However, contacts between this metal ion and RNase P have not yet been elucidated. Evidence for an inner-sphere divalent cation binding site at the tandem guanosine bases near the bulged uridine in P4 has been obtained from NMR and spectroscopic studies of a P4 stem–loop mimic, but the function of this metal ion is still unclear.[37] Data presented here reveal a critical role in activating RNase P catalytic activity for a second class of divalent cations that can form inner-sphere interactions: stabilization of a conformational change that leads to an active ES conformer (ES*). Measurements of the structural

changes that occur during this conformational change demonstrate that the position of the pre-tRNA leader relative to the P protein alters, suggesting that the substrate "docks" into the RNase P active site. These data not only elucidate a second important role for specifically bound divalent cations in the RNase P mechanism but also further our limited understanding of the structure of an active ES complex.

Divalent cation stabilizes the ES* conformation

Conformational changes are found in the kinetic pathways of a number of RNA-based enzymes,[44] including the ribosome,[45,46] group I and group II introns,[47,48] and RNase P.[23] The recently revealed conformational change in the RNase P kinetic mechanism immediately follows substrate binding and presumably optimally orients pre-tRNA in the active site for catalysis.[23] The kinetic data presented here demonstrate that an inner-sphere metal ion binds to RNase P and stabilizes the active substrate bound conformer (ES* in Scheme 2) by at least 10-fold, as indicated by the increase in pre-tRNA affinity upon addition of Ca(II). However, these kinetic and thermodynamic data do not distinguish between two possible kinetic pathways for stabilization (Scheme 3). One pathway is that the ES* conformer forms and is then stabilized by binding a divalent cation, while an alternative pathway is that the divalent cation binds to ES and facilitates the formation of the ES* conformer (Scheme 3). It is likely that the pathway depends on the divalent ion concentration, and this alteration in the kinetic pathway may partially explain the observed variability in the apparent calcium affinity (20–100 μM). At elevated concentrations, metal ions may bind to the lower-affinity metal site in E or ES prior to the conformational change, while at lower, physiological levels, the pathway in which the metal ion binds to the ES* conformer is likely favored. The details of this kinetic pathway warrant further investigation by techniques that allow for the observation of transient populations of individual molecules, such as single-molecule spectroscopy.

In contrast to many other metal binding sites in RNA,[49,50] cobalt hexammine enhances, rather than inhibits, the calcium affinity of ES*. This synergistic behavior demonstrates that cobalt hexammine stabilizes ES*Me(II) relative to ES* and ES (Scheme 3 and Fig. S2), presumably by interacting with the RNA and stabilizing the RNase P structure. Furthermore, these data suggest that the high-affinity metal site forms an inner-sphere complex. The second, weaker binding metal ion that activates the catalytic activity in RNase P (Fig. 4b) is inhibited by cobalt hexammine, demonstrating that this cationic complex competes with divalent metal ions for binding to this site.[26,51] This differential dependence on the concentration of cobalt hexammine contributes to the large difference in measured metal affinities of the two sites (~40 μM *versus* 19 mM).

Structure of ES

The first structural snapshot of the ES conformer was facilitated by the discovery that an inner-sphere metal ion is required for formation of a significant population of the ES* conformer. All previous ES models have been derived from data obtained in the presence of high levels (>10 mM) of Ca(II),[20,21,52] conditions that stabilize the ES complex in the active ES* conformer. To capture the structural changes that occur in the conformational change from the ES complex to the ES* complex, we measured changes in the distances between fluorophores on the P protein and pre-tRNA 5′ leader by trFRET as a function of the calcium concentration in the presence of cobalt hexammine. The ES complex formed in $Co(NH_3)_6$ (III) represents the ES structure, while the structure in the presence of saturating calcium, as previously reported,[20] corresponds to the ES* structure. The model of the ES complex was built (see Materials and Methods) by manually adjusting the position of the 5′ leader in the previous P protein·pre-tRNA 5′ leader model with the use of distance restrictions derived from trFRET measurements.[20] The 5′ leader was docked in the P protein, maintaining distance changes between the ES and ES* positions of the N (-5) nucleotide within 0.7 Å of the experimentally observed distance changes. The two models illustrating the relative placement of the pre-tRNA 5′ leader in the ES and ES* complexes are shown in Fig. 6. Comparison of these two models demonstrates the subtle repositioning of the 5′ leader in the ES* complex relative to the ES state as it moves toward the P protein·PRNA interface. In the initial encounter complex, the leader is situated in the central cleft and the pre-tRNA cleavage site is located near the first β-strand of the cleft. Furthermore, both models show nucleotide bases of the substrate interacting with the hydrophobic cleft of P protein, consistent with recent studies demonstrating that the fourth nucleotide in the pre-tRNA leader on the 5′ side of the cleavage site [N(-4)] contacts Y34 in P protein (*B. subtilis* numbering).[53] Accordingly, in the ES* model, the base at N(-4) is oriented to interact with Y34. The structural changes described here and illustrated in our model provide a significant step forward in understanding the structural rearrangements that accompany the formation of the active ES conformer.

Metal binding sites in the holoenzyme–substrate complex

There is currently little information available about conformational changes that occur in the PRNA subunit during ES* formation. However, a number of previously identified metal binding sites could function to stabilize the active conformer of RNase P. Biochemical and structural characterizations of *B. subtilis*, *B. stearothermophilus*, and *Escherichia coli* PRNA have identified several regions that bind metal ions potentially important to RNase P catalysis, including PRNA helices P3 and P4, as well as their joining region J3/4 (see Ref. 4 and references

therein). Helices P3 and P4 are located at the core of the catalytic PRNA and in close proximity to both the P protein and pre-tRNA, as shown by cross-linking and affinity cleavage assays.[19,21] Furthermore, helix P4 is the most conserved region of PRNA, and phosphorothioate modifications of non-bridging oxygens in the P4 helix, particularly at A49 and A50 in *B. subtilis* PRNA (A67 and A68 in *E. coli*), impair catalysis by up to 10,000-fold with minimal effects on pre-tRNA affinity.[30,32,54] Some of these catalytic defects can be rescued by adding Mn(II), suggesting that metal ions form an inner-sphere contact with the P4 helix phosphodiester backbone.[13,30,32,55] Additionally, cross-linking studies examining the position of the pre-tRNA cleavage site relative to helix P4 suggest that metal binding to helix P4 leads to indirect stabilization of catalytic metal ions at the scissile phosphate.[56] Recent studies using a combination of XAS and NMR spectroscopy identified and characterized an inner-sphere metal ion bound to the nucleotides corresponding to G378 and G379 (*B. subtilis* numbering) in a stem–loop helix mimic of *B. subtilis* helix P4.[37] The tightly bound Ca(II) or Mg(II) observed in our experiments could potentially bind to such a site in helix P4 in the ES complex to stabilize ES*. A role for particular metal-ion binding sites in stabilizing the active ES* conformer can be tested by exploring the effect of structural changes in PRNA on the conformational change.

Implications of the metal-stabilized conformational change to the RNase P mechanism

These data provide clear evidence that at least two classes of inner-sphere divalent metal ions are required for RNase P catalytic function: a high-affinity metal ion stabilizes a conformational change required for catalysis, while a lower-affinity metal ion activates catalytic activity. Previously, a two-metal-ion mechanism for activation of RNase P catalysis has been proposed where one metal-ion positions and assists in deprotonating the water nucleophile, while the second ion coordinates and stabilizes the 3′-oxygen leaving group at the cleavage site.[55,57,58] The metal ion that stabilizes the conformational change may also participate in stabilizing the transition state for cleavage. However, it is not possible to determine a catalytic role for this metal ion from the current data since the conformational change occurs prior to cleavage. Identification of the position of this metal ion relative to the pre-tRNA cleavage site should provide further insight into its function.

The ES-to-ES* transition is an essential step that occurs prior to the cleavage reaction in the kinetic mechanism of RNase P[23] (Scheme 1). Although the formation of the ES* conformer is a crucial kinetic step, it is unclear precisely what role the conformational change is playing in the RNase P catalytic pathway. There are a number of possible functions that the metal-stabilized conformational change could accomplish. For example, the formation of a high-affinity metal site after substrate binding may be a mechanism to limit catalysis of self-cleavage of the PRNA phosphodiester backbone by a reactive metal ion. Thus, the metal-dependent conformational change could confer an evolutionary advantage to the ribozyme, protecting PRNA from degradation. It could also help facilitate the proposed unwinding of the 5′ and 3′ ends of pre-tRNA prior to catalysis.[59] Additionally, the conformational change prior to cleavage may contribute to high cleavage-site fidelity by promoting specific contacts between the putative active site in PRNA and the cleavage site of pre-tRNA and may be crucial in positioning the active-site residues and magnesium-hydroxide nucleophile to catalyze hydrolysis.[21,23,60,61] Consistent with this, we observed that the ES* conformer is stabilized by a divalent cation and repositions the pre-tRNA cleavage site in close proximity to the PRNA·P protein interface. In fact, we speculate that this conformational change may act as a proofreading step to distinguish cognate from non-cognate substrates given the near-diffusion-controlled association kinetics and high substrate affinity. A similar mechanism has been proposed for EF-Tu-mediated amino-acylated tRNA selection at the A site of the ribosome.[62] Furthermore, this hypothesis is consistent with previous studies suggesting that a conformational change enhances the ability of RNase P to recognize the wide variety of pre-tRNA substrates.[63] In summary, these results provide a framework for understanding the kinetic events prior to the chemistry step in the RNase-P-catalyzed reaction that are essential for substrate selection and high catalytic efficiency.

Materials and Methods

Materials

Chemicals were purchased from commercial suppliers of the highest purity possible. NTPs were purchased from Amersham Bioscience (Piscataway, NJ) or USB (Cleveland, OH). Guanosine 5′ monothiophosphate (GMPS) was synthesized as described previously.[64] 5-Iodoacetamidofluorescein and TMR-5-iodoacetamide were purchased from Molecular Probes (Eugene, OR). Buffers were prepared using Milli-Q treated deionized water (Millipore Corporation) and degassed before each experiment. The concentration of $Co(NH_3)_6Cl_3$ was determined by absorbance using $\varepsilon_{473\ nm} = 56.2\ M^{-1}\ cm^{-1}$.[65] Prism (GraphPad Software) or Kaleidagraph (Synergy Software) was used to fit these data.

RNA and protein preparation

B. subtilis PRNA and pre-tRNA^{Asp} containing a 5-nucleotide leader sequence were prepared by *in vitro* transcription from linearized plasmids catalyzed by recombinant T7 RNA polymerase prepared using a plasmid kindly provided by Prof. W. T. McAllister.[66,67] The Fl-pre-tRNA substrates were prepared by first labeling pre-tRNA^{Asp} with a 5′ monothiophosphate. Pre-tRNA^{Asp} with a 5′ monothiophosphate was transcribed in the presence of GMPS [4 mM ATP, CTP, UTP, and GMPS, 0.8 mM GTP, 0.1 μg/μL of T7 RNA

polymerase, 0.1 μg/μL of linearized DNA template, 28 mM $MgCl_2$, 1 mM spermidine, 5 mM dithiothreitol (DTT), and 50 mM Tris [Tris-(hydroxymethyl)-aminomethane]–HCl, pH 8.0, incubated at 37 °C for 4 h]. With the use of these conditions, >80% of the pre-$tRNA^{Asp}$ substrates were labeled with 5′-GMPS. The subsequent labeling of these substrates with Fl was accomplished by incubating the 5′-GMPS-labeled substrate in the presence of 5-iodoacetamidofluorescein as described by Rueda *et al.*[20]

PRNA and pre-tRNA were purified by denaturing PAGE (7 M urea and 8% polyacrylamide).[68] RNA bands were excised from the gel and soaked in TES buffer [10 mM Tris–HCl, pH 8.0, 1 mM ethylenediaminetetraacetic acid (EDTA), and 100 mM NaCl] with 0.1% SDS overnight. The eluted RNA was exchanged into TES buffer by several iterations of concentration/dilution using centrifugal filtration (molecular mass cutoff = 10,000 Da; Amicon-Ultra, Millipore Corporation), further purified by ethanol precipitation and resuspended in water. RNase P RNA (4 μM) prepared by this method contained < 0.2 μM Ca(II) or Mg(II), as determined by inductively coupled plasma mass spectroscopy in the geology department of the University of Michigan (Ann Arbor, MI).

Variants of P protein with cysteine substituted at L94, E40, or Y113 were prepared as previously described.[52] Briefly, P proteins were expressed in *E. coli* BL21(DE3) pLysS cells and purified by CM-Sepharose ion-exchange chromatography. The protein concentrations were determined by measuring the absorbance at 280 nm in 6 M GdnHCl[69,70] using $\varepsilon_{280} = 5120\ M^{-1}\ cm^{-1}$ (wild-type P protein), $5160\ M^{-1}\ cm^{-1}$ (E40C and L94C variants), and $3900\ M^{-1}\ cm^{-1}$ (Y113C variant). P protein variants were dialyzed into 10 mM Tris, pH 8.0, 100 mM KCl, 20 mM DTT, and 10% (v/v) glycerol and stored at −80 °C.

Preparation of labeled pre-tRNA and RNase P

TMR labeling of the single-cysteine P protein mutants was performed as described previously,[20] except that DTT was replaced with 1.5 mM TCEP [tris(2-carboxyethyl) phosphine; Pierce]. The TMR labeling efficiency for the P protein variants is >60%. TMR-labeled P protein variants were used for trFRET and fluorescence stopped-flow experiments without further purification.

PRNA or Fl-pre-tRNA was denatured by incubation at 95 °C for 2 min in 10 mM Tris–HCl, pH 8.0, and 1 mM EDTA and then incubated at 37 °C for >15 min. PRNA and pre-tRNA were refolded by dilution into either cobalt hexammine [2 mM $Co(NH_3)_6Cl_3$, 189 mM KCl, 50 mM Tris, 50 mM Mes [2-(*N*-morpholino)ethanesulfonic acid], pH 6.0] or calcium (10 mM $CaCl_2$, 20 mM DTT, 150 mM KCl, 50 mM Tris, 50 mM Mes, pH 6.0) buffers and incubated at 37 °C for at least 30 min. Next, the holoenzyme was formed by addition of a stoichiometric amount of either unlabeled or TMR-labeled P protein to the PRNA, followed by incubation for 30 min at 37 °C.[20,23] The ES complex was formed by adding folded Fl-pre-$tRNA^{Asp}$ to the holoenzyme in buffer containing 2 mM $Co(NH_3)_6{\cdot}Cl_3$ and incubated for >15 min at 25 °C.

Pre-tRNA binding affinity determined by fluorescence titration

Fluorescence titrations were performed by titrating RNase P into Fl-pre-tRNA on an Eclipse spectrofluorometer (Varian Corporation) and monitoring the fluorescence intensity of Fl ($\lambda_{ex} = 488$ nm, $\lambda_{em} = 524$ nm; 5-nm bandpass) either in 2 mM $Co(NH_3)_6Cl_3$, 189 mM KCl, 50 mM Tris, 50 mM Mes, pH 6.0, at 25 °C, and varying concentrations of $CaCl_2$ or in 10 mM $CaCl_2$, 20 mM DTT, 150 mM KCl, 50 mM Tris, and 50 mM Mes, pH 6.0, at 25 °C. The KCl concentration was altered to account for differences in ionic strength between the assays with $Co(NH_3)_6Cl_3$ and $CaCl_2$. The fluorescence intensity was corrected for dilution and background fluorescence and then normalized to that of the free substrate, as described previously.[71] The dissociation constant (K_d) was obtained by fitting the concentration dependence of the observed relative fluorescence enhancement, ΔF, with a binding isotherm for a 1:1 complex that accounts for changes in the concentrations of pre-tRNA and RNase P (Eq. (1)), where E and S are the total enzyme and substrate concentrations, respectively:

$$\Delta F = \Delta F_0 + (\Delta F_{max} - \Delta F_0) \times \frac{\left((K_d + [E] + [S]) - \sqrt{(K_d + [E] + [S])^2 - 4[E][S]}\right)}{2[S]} \quad (1)$$

The pre-tRNA affinity of RNase P in 2 mM cobalt hexammine was determined at several concentrations of calcium. The apparent dissociation constant for calcium was determined by fitting these data to a binding isotherm that allows for cooperative dependence on the calcium concentration (Eq. (2)) or for calcium binding to both E and ES (Eq. (3)). The calcium affinity was also determined by titrating $CaCl_2$ into the preformed RNase P·Fl-pre-tRNA complex (300 nM RNase P, 15 nM Fl-pre-tRNA in 50 mM Tris, 50 mM Mes, 2 mM cobalt hexammine, 20 mM DTT, and 380 mM KCl, pH 6.0, at 25 °C) and measuring the fluorescence intensity of Fl after equilibration for 5 min. The apparent metal dissociation constant was calculated from the divalent ion concentration dependence of the fluorescent enhancement by fitting Eq. (4) to the data where ΔF is the observed fluorescence enhancement, ΔF_{max} is the maximal fluorescent enhancement, K_{Ca} is the apparent dissociation constant for calcium, and n is the apparent cooperativity factor.

$$K_{d,obs} = K_{d,CoHex} / (1 + [Ca(II)]^n / (K_{Ca})^n) \quad (2)$$

$$K_{d,obs} = K_{d,CoHex}\left(1 + [Ca(II)] / K_{Ca,E}\right) / \left(1 + [Ca(II)] / K_{Ca,ES}\right) \quad (3)$$

$$\Delta F = \Delta F_{max} / (1 + [Ca(II)]^n / (K_{Ca})^n) \quad (4)$$

Binding kinetics by fluorescence stopped-flow techniques

Fluorescence stopped-flow measurements were carried out on a model SF-2001 stopped-flow spectrofluorometer (KinTek Corp., Austin, TX) fitted with a 75W Xe-arc lamp. Fl was excited at 488 nm (slit width, 0.1–2 mm). Fl fluorescence emission was monitored using a long-pass filter (>500 nm; Corion, LL-500-F), and FRET to the TMR attached to the E40C P protein was observed using a 600-nm cut-on filter (Corion, LL-600-F). All kinetic traces were an average of five to eight independent determinations. Time-dependent fluorescence traces were analyzed by fitting multiple exponentials to the data (Eq. (5)) to obtain the fluorescence amplitude (A) and the observed rate

constant (k_{obs}) for each exponential phase, where $F(0)$ is the initial fluorescence intensity and t is time:

$$F(t) = \sum A_n\left[1 - \exp\left(-k_{obs,n}t\right) + F(0)\right] \quad (5)$$

Single-turnover cleavage of Fl-tRNA catalyzed by RNase P

The TMR-E40C RNase P·Fl-pre-tRNA complex (35 nM Fl-pre-tRNA, 125 nM RNase P) was prepared in 2 mM cobalt hexammine, 189 mM KCl, 50 mM Tris, and 50 mM Mes, pH 6.0, at 25 °C. The reaction was initiated by addition of $MgCl_2$ (0–50 mM) and stopped by addition of 50 mM EDTA and 5 M urea using either a chemical quench-flow apparatus (KinTek Corp.) or by hand. Cleavage of Fl-pre-tRNA was analyzed by denaturing PAGE and quantified using a STORM 980 fluorescence scanner (Molecular Dynamics). The single-turnover rate constants (k_{obs}) were obtained by fitting a first-order exponential equation (Eq. (5)) to the fraction of substrate cleaved as a function of time. The apparent dissociation constant for Mg(II) was determined by fitting a rectangular hyperbola to the magnesium dependence of k_{obs}.

Distance measurement by trFRET

The position of the 5′ leader of pre-tRNA^{Asp} relative to the *B. subtilis* P protein in RNase P was probed by trFRET, as described previously.[20,72] The TMR-RNase P·Fl-pre-tRNA complex (1 μM Fl-pre-tRNA, 2 μM TMR-RNase P) was prepared in 2 mM cobalt hexammine, 189 mM KCl, 50 mM Tris, and 50 mM Mes, pH 6.0, at 25 °C. The Fl emission decay of the donor-only complex was measured and fit with a sum of three exponential decays characterized by their lifetime (τ_i) and relative amplitude (R_i), as previously described.[20,72,73] Likewise, the doubly labeled holoenzyme–substrate complex was formed using the TMR-labeled single-cysteine P protein mutants. The Fl emission decay, $I_{DA}(t)$, was then measured in the presence of the acceptor fluorophore in the TMR-RNase P·Fl-pre-tRNA complex, and Eq. (6) was fit to these data, where τ_i and α_i are the singly labeled lifetime parameters, R_0 is the Förster distance for 50% energy transfer (55 Å for the Fl-TMR pair),[74] and $P(R)$ is the distance distribution. The latter was modeled as a three-dimensional weighted Gaussian (Eq. (7)), where σ and μ describe the shape of the Gaussian and N is a normalization constant. An additional adjustable parameter was the fraction of singly labeled component (typically 30%–45%), caused by unbound Fl-pre-tRNA, or P protein without an acceptor fluorophore. In these experiments, the contributions from singly labeled and doubly labeled complexes were accurately distinguished, as confirmed by deliberately spiking the sample with singly labeled material and still recovering the same distance distribution. An instrument function was systematically measured using a dilute solution of non-dairy creamer as scattering solution to deconvolute the fluorescence decays before fitting the data.

$$I_{DA}(t) = \int P(R)\sum_i \alpha_i \exp\left(-\frac{t}{\tau_i}\left[1 + \left(\frac{R_0}{R}\right)^6\right]\right)dR \quad (6)$$

$$P(R) = 4\pi R^2 N \exp\left(-\sigma(R-\mu)^2\right) \quad (7)$$

Models of the ES and ES* complexes

Models of the position of the 5′ leader of pre-tRNA with respect to the P protein in the ES and ES* complexes were built using the software package PyMOL†.[75] The editing tools built in PyMOL were used to manually adjust the position of the 5′ leader in the previous P protein·pre-tRNA 5′ leader model derived from trFRET measurements.[20] The distances between the α-phosphate of the N(-5) nucleobase in the leader and the γ-carbon of side chains of E40, L94, and Y113 were determined using the measurement wizard in PyMOL. The ES* complex was modeled first, starting with the structure of the previously reported pre-tRNA leader using the trFRET distances reported by Rueda *et al.*[20] and those measured here (Fig. 5). The length of the linker between the Fl moiety and P protein amino acids was estimated to be 10 Å. In this case, the bases were repositioned to interact with the protein, as indicated by the N(-4)·Y34 contact.[53] The ES complex was modeled from the ES* complex model. The 5′ leader in this complex was repositioned so that the distance changes between the ES position and the ES* position of the N(-5) nucleotide were within 0.7 Å of the experimentally observed distance changes.

Acknowledgements

This work was supported by funding from the National Institutes of Health (grant GM55387 to C.A.F., grant T32 GM08353 to K.S.K., and grant GM062357 to N.G.W.). We thank Dr. Anthony Manzo for helping with the trFRET measurements.

Supplementary Data

Supplementary data associated with this article can be found, in the online version, at doi:10.1016/j.jmb.2010.04.050

References

1. Pyle, A. M. (2002). Metal ions in the structure and function of RNA. *J. Biol. Inorg. Chem.* **7**, 679–690.
2. Misra, V. K. & Draper, D. E. (1998). On the role of magnesium ions in RNA stability. *Biopolymers*, **48**, 113–135.
3. Ye, J. D., Tereshko, V., Frederiksen, J. K., Koide, A., Fellouse, F. A., Sidhu, S. S. *et al.* (2008). Synthetic antibodies for specific recognition and crystallization of structured RNA. *Proc. Natl Acad. Sci. USA*, **105**, 82–87.
4. Kazantsev, A. V., Krivenko, A. A. & Pace, N. R. (2009). Mapping metal-binding sites in the catalytic domain of bacterial RNase P RNA. *RNA*, **15**, 266–276.
5. Tanaka, Y., Kasai, Y., Mochizuki, S., Wakisaka, A., Morita, E. H., Kojima, C. *et al.* (2004). Nature of the chemical bond formed with the structural metal ion at the A9/G10.1 motif derived from hammerhead ribozymes. *J. Am. Chem. Soc.* **126**, 744–752.

† http://www.pymol.org

6. Draper, D. E., Grilley, D. & Soto, A. M. (2005). Ions and RNA folding. *Annu. Rev. Biophys. Biomol. Struct.* **34**, 221–243.
7. Draper, D. E. & Misra, V. K. (1998). RNA shows its metal. *Nat. Struct. Biol.* **5**, 927–930.
8. Frederiksen, J. K. & Piccirilli, J. A. (2009). Identification of catalytic metal ion ligands in ribozymes. *Methods*, **49**, 148–166.
9. Smith, J. K., Hsieh, J. & Fierke, C. A. (2007). Importance of RNA–protein interactions in bacterial ribonuclease P structure and catalysis. *Biopolymers*, **87**, 329–338.
10. Record, M. T., Jr., Lohman, M. L. & De Haseth, P. (1976). Ion effects on ligand–nucleic acid interactions. *J. Mol. Biol.* **107**, 145–158.
11. Woodson, S. A. (2005). Metal ions and RNA folding: a highly charged topic with a dynamic future. *Curr. Opin. Chem. Biol.* **9**, 104–109.
12. Kirsebom, L. A. & Trobro, S. (2009). RNase P RNA-mediated cleavage. *IUBMB Life*, **61**, 189–200.
13. Harris, M. E. & Christian, E. L. (2003). Recent insights into the structure and function of the ribonucleoprotein enzyme ribonuclease P. *Curr. Opin. Struct. Biol.* **13**, 325–333.
14. Torres-Larios, A., Swinger, K. K., Krasilnikov, A. S., Pan, T. & Mondragon, A. (2005). Crystal structure of the RNA component of bacterial ribonuclease P. *Nature*, **437**, 584–587.
15. Kazantsev, A. V., Krivenko, A. A., Harrington, D. J., Holbrook, S. R., Adams, P. D. & Pace, N. R. (2005). Crystal structure of a bacterial ribonuclease P RNA. *Proc. Natl Acad. Sci. USA*, **102**, 13392–13397.
16. Kazantsev, A. V., Krivenko, A. A., Harrington, D. J., Carter, R. J., Holbrook, S. R., Adams, P. D. & Pace, N. R. (2003). High-resolution structure of RNase P protein from *Thermotoga maritima*. *Proc. Natl Acad. Sci. USA*, **100**, 7497–7502.
17. Stams, T., Niranjanakumari, S., Fierke, C. A. & Christianson, D. W. (1998). Ribonuclease P protein structure: evolutionary origins in the translational apparatus. *Science*, **280**, 752–755.
18. Spitzfaden, C., Nicholson, N., Jones, J. J., Guth, S., Lehr, R., Prescott, C. D. *et al.* (2000). The structure of ribonuclease P protein from *Staphylococcus aureus* reveals a unique binding site for single-stranded RNA. *J. Mol. Biol.* **295**, 105–115.
19. Buck, A. H., Kazantsev, A. V., Dalby, A. B. & Pace, N. R. (2005). Structural perspective on the activation of RNase P RNA by protein. *Nat. Struct. Mol. Biol.* **12**, 958–964.
20. Rueda, D., Hsieh, J., Day-Storms, J. J., Fierke, C. A. & Walter, N. G. (2005). The 5′ leader of precursor $tRNA^{Asp}$ bound to the *Bacillus subtilis* RNase P holoenzyme has an extended conformation. *Biochemistry*, **44**, 16130–16139.
21. Niranjanakumari, S., Day-Storms, J. J., Ahmed, M., Hsieh, J., Zahler, N. H., Venters, R. A. & Fierke, C. A. (2007). Probing the architecture of the *B. subtilis* RNase P holoenzyme active site by crosslinking and affinity cleavage. *RNA*, **13**, 512–535.
22. Massire, C., Jaeger, L. & Westhof, E. (1998). Derivation of the three-dimensional architecture of bacterial ribonuclease P RNAs from comparative sequence analysis. *J. Mol. Biol.* **279**, 773–793.
23. Hsieh, J. & Fierke, C. A. (2009). Conformational change in the *Bacillus subtilis* RNase P holoenzyme–pre-tRNA complex enhances substrate affinity and limits cleavage rate. *RNA*, **15**, 1565–1577.
24. Crary, S. M., Niranjanakumari, S. & Fierke, C. A. (1998). The protein component of *Bacillus subtilis* ribonuclease P increases catalytic efficiency by enhancing interactions with the 5′ leader sequence of pre-$tRNA^{Asp}$. *Biochemistry*, **37**, 9409–9416.
25. Kurz, J. C. & Fierke, C. A. (2000). Ribonuclease P: a ribonucleoprotein enzyme. *Curr. Opin. Chem. Biol.* **4**, 553–558.
26. Kurz, J. C. & Fierke, C. A. (2002). The affinity of magnesium binding sites in the *Bacillus subtilis* RNase P-pre-tRNA complex is enhanced by the protein subunit. *Biochemistry*, **41**, 9545–9558.
27. Cassano, A. G., Anderson, V. E. & Harris, M. E. (2004). Analysis of solvent nucleophile isotope effects: evidence for concerted mechanisms and nucleophilic activation by metal coordination in nonenzymatic and ribozyme-catalyzed phosphodiester hydrolysis. *Biochemistry*, **43**, 10547–10559.
28. Fang, X. W., Pan, T. & Sosnick, T. R. (1999). Mg^{2+}-dependent folding of a large ribozyme without kinetic traps. *Nat. Struct. Biol.* **6**, 1091–1095.
29. Fang, X. W., Thiyagarajan, P., Sosnick, T. R. & Pan, T. (2002). The rate-limiting step in the folding of a large ribozyme without kinetic traps. *Proc. Natl Acad. Sci. USA*, **99**, 8518–8523.
30. Crary, S. M., Kurz, J. C. & Fierke, C. A. (2002). Specific phosphorothioate substitutions probe the active site of *Bacillus subtilis* ribonuclease P. *RNA*, **8**, 933–947.
31. Kaye, N. M., Zahler, N. H., Christian, E. L. & Harris, M. E. (2002). Conservation of helical structure contributes to functional metal ion interactions in the catalytic domain of ribonuclease P RNA. *J. Mol. Biol.* **324**, 429–442.
32. Christian, E. L., Kaye, N. M. & Harris, M. E. (2000). Helix P4 is a divalent metal ion binding site in the conserved core of the ribonuclease P ribozyme. *RNA*, **6**, 511–519.
33. Loria, A. & Pan, T. (2001). Modular construction for function of a ribonucleoprotein enzyme: the catalytic domain of *Bacillus subtilis* RNase P complexed with *B. subtilis* RNase P protein. *Nucleic Acids Res.* **29**, 1892–1897.
34. Frank, D. N., Ellington, A. E. & Pace, N. R. (1996). *In vitro* selection of RNase P RNA reveals optimized catalytic activity in a highly conserved structural domain. *RNA*, **2**, 1179–1188.
35. Frank, D. N. & Pace, N. R. (1997). *In vitro* selection for altered divalent metal specificity in the RNase P RNA. *Proc. Natl Acad. Sci. USA*, **94**, 14355–14360.
36. Getz, M. M., Andrews, A. J., Fierke, C. A. & Al-Hashimi, H. M. (2007). Structural plasticity and Mg^{2+} binding properties of RNase P P4 from combined analysis of NMR residual dipolar couplings and motionally decoupled spin relaxation. *RNA*, **13**, 251–266.
37. Koutmou, K. S., Casiano-Negroni, A., Getz, M. M., Pazicni, S., Andrews, A. J., Penner-Hahn, J. E. *et al.* (2010). NMR and XAS reveal an inner-sphere metal binding site in the P4 helix of the metallo-ribozyme ribonuclease P. *Proc. Natl Acad. Sci. USA*, **107**, 2479–2484.
38. Beebe, J. A., Kurz, J. C. & Fierke, C. A. (1996). Magnesium ions are required by *Bacillus subtilis* ribonuclease P RNA for both binding and cleaving precursor $tRNA^{Asp}$. *Biochemistry*, **35**, 10493–10505.
39. Smith, D., Burgin, A. B., Haas, E. S. & Pace, N. R. (1992). Influence of metal ions on the ribonuclease P reaction. Distinguishing substrate binding from catalysis. *J. Biol. Chem.* **267**, 2429–2436.
40. Hsieh, J., Walker, S. C., Fierke, C. A. & Engelke, D. R. (2009). Pre-tRNA turnover catalyzed by the yeast

nuclear RNase P holoenzyme is limited by product release. *RNA*, **15**, 224–234.
41. Cowan, J. A. (1993). Metallobiochemistry of RNA. Co $(NH_3)_6^{3+}$ as a probe for $Mg^{2+}{}_{aq}$ binding sites. *J. Inorg. Biochem.* **49**, 171–175.
42. Day-Storms, J. J., Niranjanakumari, S. & Fierke, C. A. (2004). Ionic interactions between PRNA and P protein in *Bacillus subtilis* RNase P characterized using a magnetocapture-based assay. *RNA*, **10**, 1595–1608.
43. Warnecke, J. M., Held, R., Busch, S. & Hartmann, R. K. (1999). Role of metal ions in the hydrolysis reaction catalyzed by RNase P RNA from *Bacillus subtilis*. *J. Mol. Biol.* **290**, 433–445.
44. Doherty, E. A. & Doudna, J. A. (2001). Ribozyme structures and mechanisms. *Annu. Rev. Biophys. Biomol. Struct.* **30**, 457–475.
45. Lodmell, J. S. & Dahlberg, A. E. (1997). A conformational switch in *Escherichia coli* 16S ribosomal RNA during decoding of messenger RNA. *Science*, **277**, 1262–1267.
46. Wilson, K. S. & Noller, H. F. (1998). Molecular movement inside the translational engine. *Cell*, **92**, 337–349.
47. Shan, S. O. & Herschlag, D. (2002). Dissection of a metal-ion-mediated conformational change in *Tetrahymena* ribozyme catalysis. *RNA*, **8**, 861–872.
48. Costa, M., Deme, E., Jacquier, A. & Michel, F. (1997). Multiple tertiary interactions involving domain II of group II self-splicing introns. *J. Mol. Biol.* **267**, 520–536.
49. Gong, B., Chen, J. H., Bevilacqua, P. C., Golden, B. L. & Carey, P. R. (2009). Competition between $Co(NH_3)_6^{3+}$ and inner sphere Mg^{2+} ions in the HDV ribozyme. *Biochemistry*, **48**, 11961–11970.
50. Horton, T. E. & DeRose, V. J. (2000). Cobalt hexammine inhibition of the hammerhead ribozyme. *Biochemistry*, **39**, 11408–11416.
51. Cuzic, S. & Hartmann, R. K. (2005). Studies on *Escherichia coli* RNase P RNA with Zn^{2+} as the catalytic cofactor. *Nucleic Acids Res.* **33**, 2464–2474.
52. Niranjanakumari, S., Stams, T., Crary, S. M., Christianson, D. W. & Fierke, C. A. (1998). Protein component of the ribozyme ribonuclease P alters substrate recognition by directly contacting precursor tRNA. *Proc. Natl Acad. Sci. USA*, **95**, 15212–15217.
53. Koutmou, K. S., Zahler, N. H., Kurz, J. C., Campbell, F. E., Harris, M. E. & Fierke, C. A. (2010). Protein–precursor tRNA contact leads to sequence-specific recognition of 5′ leaders by bacterial ribonuclease P. *J. Mol. Biol.* **396**, 195–208.
54. Harris, M. E. & Pace, N. R. (1995). Identification of phosphates involved in catalysis by the ribozyme RNase P RNA. *RNA*, **1**, 210–218.
55. Sun, L. & Harris, M. E. (2007). Evidence that binding of C5 protein to P RNA enhances ribozyme catalysis by influencing active site metal ion affinity. *RNA*, **13**, 1505–1515.
56. Christian, E. L., Smith, K. M., Perera, N. & Harris, M. E. (2006). The P4 metal binding site in RNase P RNA affects active site metal affinity through substrate positioning. *RNA*, **12**, 1463–1467.
57. Steitz, T. A. & Steitz, J. A. (1993). A general two-metal-ion mechanism for catalytic RNA. *Proc. Natl Acad. Sci. USA*, **90**, 6498–6502.
58. Warnecke, J. M., Furste, J. P., Hardt, W. D., Erdmann, V. A. & Hartmann, R. K. (1996). Ribonuclease P (RNase P) RNA is converted to a Cd^{2+}-ribozyme by a single Rp-phosphorothioate modification in the precursor tRNA at the RNase P cleavage site. *Proc. Natl Acad. Sci. USA*, **93**, 8924–8928.
59. Pomeranz Krummel, D. A., Kent, O., MacMillan, A. M. & Altman, S. (2000). Evidence for helical unwinding of an RNA substrate by the RNA enzyme RNase P: use of an interstrand disulfide crosslink in substrate. *J. Mol. Biol.* **295**, 1113–1118.
60. Loria, A. & Pan, T. (1999). The cleavage step of ribonuclease P catalysis is determined by ribozyme–substrate interactions both distal and proximal to the cleavage site. *Biochemistry*, **38**, 8612–8620.
61. Brannvall, M., Kikovska, E., Wu, S. & Kirsebom, L. A. (2007). Evidence for induced fit in bacterial RNase P RNA-mediated cleavage. *J. Mol. Biol.* **372**, 1149–1164.
62. Blanchard, S. C., Gonzalez, R. L., Kim, H. D., Chu, S. & Puglisi, J. D. (2004). tRNA selection and kinetic proofreading in translation. *Nat. Struct. Mol. Biol.* **11**, 1008–1014.
63. Sun, L., Campbell, F. E., Zahler, N. H. & Harris, M. E. (2006). Evidence that substrate-specific effects of C5 protein lead to uniformity in binding and catalysis by RNase P. *EMBO J.* **25**, 3998–4007.
64. Behrman, E. (2000). An improved synthesis of guanosine 5′-monothiophosphate. *J. Chem. Res.* **S**, 446–447.
65. Deng, H. & Bloomfield, V. A. (1999). Structural effects of cobalt-amine compounds on DNA condensation. *Biophys. J.* **77**, 1556–1561.
66. Milligan, J. F. & Uhlenbeck, O. C. (1989). Synthesis of small RNAs using T7 RNA polymerase. *Methods Enzymol.* **180**, 51–62.
67. He, B., Rong, M., Lyakhov, D., Gartenstein, H., Diaz, G., Castagna, R. *et al.* (1997). Rapid mutagenesis and purification of phage RNA polymerases. *Protein Expression Purif.* **9**, 142–151.
68. Kurz, J. C., Niranjanakumari, S. & Fierke, C. A. (1998). Protein component of *Bacillus subtilis* RNase P specifically enhances the affinity for precursor-$tRNA^{Asp}$. *Biochemistry*, **37**, 2393–2400.
69. Edelhoch, H. (1967). Spectroscopic determination of tryptophan and tyrosine in proteins. *Biochemistry*, **6**, 1948–1954.
70. Gill, S. C. & von Hippel, P. H. (1989). Calculation of protein extinction coefficients from amino acid sequence data. *Anal. Biochem.* **182**, 319–326.
71. Lohman, T. M. & Mascotti, D. P. (1992). Thermodynamics of ligand–nucleic acid interactions. *Methods Enzymol.* **212**, 400–424.
72. Walter, N. G. (2001). Structural dynamics of catalytic RNA highlighted by fluorescence resonance energy transfer. *Methods*, **25**, 19–30.
73. Rueda, D., Wick, K., McDowell, S. E. & Walter, N. G. (2003). Diffusely bound Mg^{2+} ions slightly reorient stems I and II of the hammerhead ribozyme to increase the probability of formation of the catalytic core. *Biochemistry*, **42**, 9924–9936.
74. Walter, N. G., Burke, J. M. & Millar, D. P. (1999). Stability of hairpin ribozyme tertiary structure is governed by the interdomain junction. *Nat. Struct. Biol.* **6**, 544–549.
75. DeLano, W. L. (2002). *The PyMOL Molecular Graphics System.* DeLano Scientific, San Carlos, CA.